Plasmonics (2023) 18:175–182
https://doi.org/10.1007/s11468-022-01736-2

Silver Nanoparticles Amplified Visible and Infrared Photoluminescence Features of Er^{3+} Ions Activated in Borate Glasses

Kempaiah Keshavamurthy[1] · Gangareddy Jagannath[2] · Dalal Abdullah Aloraini[3] · Aljawhara H. Almuqrin[3] · M. I. Sayyed[4,5] · K. N. Sathish[6] · P. Ramesh[7]

Received: 17 July 2022 / Accepted: 26 October 2022 / Published online: 7 December 2022

Abstract

Rare earth (RE)–doped glasses with high quantum efficiency and strong photoluminescence (PL) characteristics are essential for next generation photonic and optoelectronic devices. To attain strong PL emission and related attributes of Er^{3+}-doped in glass system, the silver nanoparticles (NPs) were embedded. UV-Vis absorption and microscopic measurements divulged the existence of metallic silver NPs. The PL emission of Er^{3+}-doped in titled glasses was improved in visible and infrared spectral ranges as $AgNO_3$ concentration escalated to higher level. In addition, the quantum efficiency also enhanced as the $AgNO_3$ doping level escalated to a higher level. The enhancements in PL emission intensity and quantum efficiency were ascribed to the local field induced by surface plasmons of Ag NPs. The outcomes suggest that the high concentration of Ag NPs routed in Er^{3+}-doped glass system is useful in fabricating the optical amplifiers and solid-state lasers.

Keywords Antimony trioxide · Nanoparticles · Borate oxide glasses · Erbium ions · Photonic applications

Introduction

Metal nanoparticles (NPs) routed in different optically transparent hosts such as polymers [1], silica films [2], colloidal solutions [3], and glasses [2] are of enormous curiosity to the scientific community owing to their potential functionalities in bio-sensing [4], bio-imaging [5], molecular species sensing by surface-enhanced scattering spectroscopy [6], plasmonics [7], luminescence [8], and nonlinear optical [9]. Among all other hosts for routing the metal NPs, the glass hosts are exceptionally attractive because of high metal solubility along with uniform distribution, which allows for the tuning of optical and other properties of hosts based on the NPs concentration [2]. In particular, the metal NPs embedment in rare earth (RE) containing glass matrices is significantly attracted the research community for tuning the photoluminescence (PL) and quantum efficiency magnitudes of RE^{3+} ions loaded in glass specimens [10]. Usually when the RE concentration is increased in the composition to tune the PL and related parameters, at higher concentration of RE ions, the properties are deteriorated due to concentration quenching effect which limits their practical use in the devices. By embedding NPs to RE-activated glasses provides an alternative way to tune the PL and related attributes significantly without immediate quenching in the properties which are

✉ Gangareddy Jagannath
jagannathgreddy@gmail.com

✉ P. Ramesh
prameshklr@gmail.com

[1] Department of Physics, Dayananda Sagar College of Engineering, Bengaluru 560078, India

[2] Department of Post–Graduate Studies and Research in Physics, The National College, Jayanagar, Bengaluru 560070, Karnataka, India

[3] Department of Physics, College of Science, Princess Nourah Bint Abdulrahman University, PO Box 84428, Riyadh 11671, Saudi Arabia

[4] Department of Physics, Faculty of Science, Isra University, Amman, Jordan

[5] Department of Nuclear Medicine Research, Institute for Research and Medical Consultations (IRMC), Imam Abdulrahman Bin Faisal University (IAU), P.O. Box 1982, Dammam 31441, Saudi Arabia

[6] Department of Physics, Govt. First Grade College, Chickaballapur 562101, India

[7] Department of Physics, Govt. College for Women, Chintamani 563125, India

desired for specific applications. The co-doping of a small quantity of metal NPs to the optimized glass composition significantly improves the PL and other optical features by the local electric field modified [11–13] and/or transfer of energy (from NPs to RE ions) phenomena [11, 14]. This luminescence enhancement of RE ions due to the inclusion of NPs in the composition was first observed by Malta et al. [15] in 1985 for Eu^{3+} ions–doped materials with co-doping of silver (Ag) NPs. Then onwards, this method has been widely followed by many glass researchers for developing the glassy materials for photonic applications [16–20] by achieving significant enhancement in PL properties of RE-doped glasses, and different attributions were proposed for the observed enhancement. Few examples are as follows: Silva et al. [16] have achieved the luminous up conversion enhancement in Er^{3+}-loaded PbO–GeO_2 glass specimens by co-doping with Ag NPs and highlighted that the enhancement was due to local field effect. Dousti et al. [17] have observed the improved emission curves of Er^{3+} activated heavy metal oxide vitreous systems caused by the surface plasmon resonance (SPR) of silver NPs. Jiani et al. [18] have shown the significant fluorescence amplification of trivalent erbium ions in silver NPs co-doped B_2O_3–Bi_2O_3–TiO_2 glass system and highlighted due to both the energy transfer and local field effects. The contribution of Ag NPs on the 1.5 µm emission amplification of trivalent erbium ions activated in complex silicate based glass has recently been examined by Rajaramakrishna et al. [20] and underlined the local electric field evinced and energy transfer routes are the acceptable claims for emission gained by the Er^{3+} ions.

Notably, among numerous glass families of interest, the borate vitreous compositions have attracted the scientific community for photonic applications since the borate matrix can dissolve high amounts of RE ions and NPs [21, 22]. In addition, the borate glasses possess wide transparency from visible to infrared regions, strong thermo–chemico–mechanical stability, and low glass transition temperatures [22]. Furthermore, the inclusion of high molar mass oxides in a borate glass system greatly decreases the energy of phonons present in the host and improves the PL intensity of RE ions by reducing non-radiative emissions [23]. The Sb_2O_3 is one of the high molar mass oxides, and it also serves as the thermal reducing agent to obtain Ag^0 NPs from its ionic state [24]. Therefore, the selection of Sb_2O_3 in the glass composition provides a straightforward, low-cost strategy to fabricate metal NPs containing glasses without following additional heat treatments at different temperatures or for different durations. Among all RE ions, the Er^{3+} ion is one of the most promising RE ions in the lanthanide group since it possesses a favorable energy level scheme to be exploited in a wide variety of applications which includes solid-state lasers, microchip lasers, eye safe lasers, and many other advanced photonic systems [25, 26].

Thus, Er^{3+} loaded in glass specimens has received significant attention as an active host for lasers, upconverters, amplifiers, and so forth. It was identified that only a few investigations are found in the open literature with improvement in 1.53 µm band PL emission by the inclusion of metal NPs in the glass hosts [25, 27–30]. The current investigation aims to prepare Er^{3+}-activated borate-based glasses embedded with silver NPs to enhance PL emission at the 1.53 µm emission band and in the visible region. The efficacy of silver NPs concentration on spectroscopic and PL attributes of Er^{3+} ions has been analyzed, and the mechanism trustworthy for enhancement of PL and related attributes has been discussed in detail.

Materials and Methods

The glass specimens bearing the compositional formula of (mol %) $10Sb_2O_3$–$20Na_2O$–$69B_2O_3$–$1Er_2O_3$–$xAgNO_3$ ($x = 0 - 0.8$ mol %) were fabricated through the melting and quenching process. Before proceeding for characterization, the fabricated glass specimens were designated as Er1Ag–x; in the codes, the "x" indicates the $AgNO_3$ content added in the composition to obtain the Ag NPs. The glass free from Er_2O_3 and Ag NPs was coded as Er0Ag–0. The glass compositional mixtures of 30 g were kept in a high-temperature furnace by loading into the porcelain crucibles. The mixtures were melted at 950 °C and rapidly quenched on pre-annealed brass plates. After the quenching, immediatley the glasses were moved to annealing furnace that was already programmed with 350 °C for 4 h. This process was used to remove internal stress in the glass samples that had developed during quick quenching from high temperatures. X-ray diffraction (XRD) profiles with 2θ range from 10 to 90° of step size of 0.05° were recorded using Rigaku Ultima IV X-ray diffractometer. The optical absorbance spectra were collected utilizing Carry 5000 UV–Vis–NIR spectrophotometer from 200 to 1700 nm. The presence and morphology of Ag NPs in the Er1Ag–0.2 glass specimen were divulged by transmission electron microscopy (TEM) micrograph captured with the help of FEI Technai G2 20 TEM. The photonic measurements of all the glasses were recorded using an Edinburg Spectro Fluorimeter (FLS 980) provided with flash lamp (xenon) as the source of excitation.

Results and Discussion

The XRD profiles Er1Ag–0, Er1Ag–0.2, and Er1Ag–0.8 glass samples are presented in Fig. 1. The observed broad diffused hump with no sharp crystallization peak suggests the missing of long-range atomic arrangement in the studied glasses. These signatures also affirm the non-crystalline

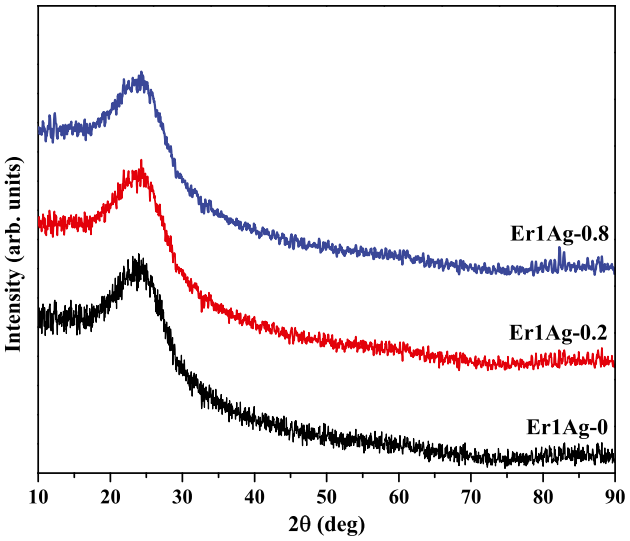

Fig. 1 XRD results of some of the investigated glasses

characteristic of the glass specimens examined in the current work. The TEM micrograph of the Er1Ag–0.2 glass is displayed in Fig. 2a. The size distribution of silver NPs and the average nanoparticle diameter were analyzed utilizing ImageJ computer software. The size of the Ag NPs computed utilizing ImageJ software has been plotted as a histogram and presented in Fig. 2b. The histogram profile reveal the size of metallic silver NPs lies in the range of 2.50 - 12.46 nm, with 7.78 nm median size. The TEM image displayed in Fig. 2a also unveils that the silver NPs embedded in Er1Ag–0.2 glass are spherical in form and are distributed uniformly in the sample. Additionally, the TEM image of the Er1Ag–0.2 glass host shows some Ag NPs with non-spherical shapes.

The selective formation of Ag^0 NPs from their counter ionic species has been occurred in the current system based on the following thermochemical equations [31],

$$Sb^{5+}/Sb^{3+}(E^0 = 0.586V) \quad (1)$$

$$Ag^{+}/Ag^{0}\ (E^0 = 0.801V) \quad (2)$$

$$Er^{3+}/Er^{0}(E^0 = -2.306V) \quad (3)$$

The reaction, i.e., $Sb^{3+} + 2Ag^{+} \rightarrow Sb^{5+} + 2Ag^{0}$, has the $E^0 = 1.02$ V and the $\Delta G = -197$ kJ. These magnitude of E^0 and ΔG divulge the reaction is plausible to induce in the system. However, the reaction $3Sb^{3+} + 2Er^{3+} \rightarrow 3Sb^{5+} + 2Er^{0}$ owes the $E^0 = -5.76$ V and the $\Delta G = 3334$ kJ, the negative sign on E^0 and positive magnitude of ΔG clearly suggest that the later reaction is not plausible to induce in the currently investigated glass system. These two reactions and their inferences clearly unveil the antimony selectively reducing Ag^{+} to Ag^{0} (first reduction reaction) and not reducing Er^{3+} to Er^{0} (second reduction reaction) in the glass matrix considered in the current investigation.

Optical absorption spectra of Er1Ag–0 (doped with only 1 mol % of Er_2O_3 and free from Ag NPs), Er1Ag–0.2, and Er1Ag–0.8 glass specimens in the range of 200–1700 nm are displayed in Fig. 3. The inset of Fig. 3 displays the absorption spectra of Er0Ag–0 (free from Er_2O_3 and Ag NPs) and Er1Ag–0 glasses with designation to the absorption peaks observed in Er1Ag–0 glass. The noticed Er^{3+}

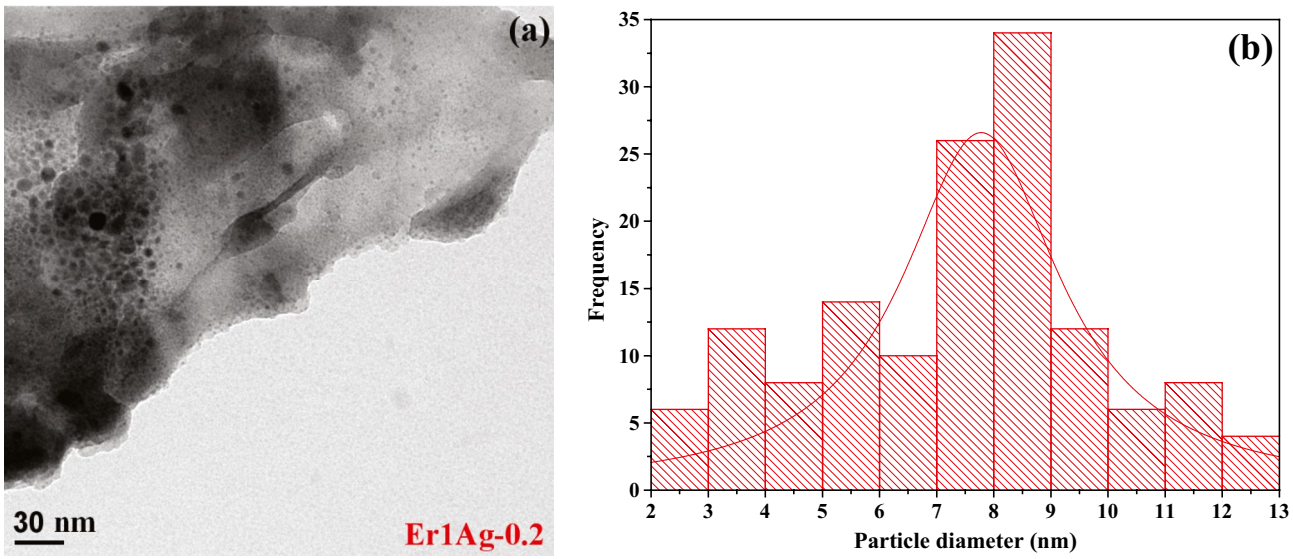

Fig. 2 TEM image of Er1Ag–0.2 glass **(a)** and corresponding Ag NPs size variation profile **(b)** in the tested glass

characteristic absorption peaks were assigned be referring the articles [25, 31]. The spectrum of Er0Ag–0 glass does not demonstrate any absorption peaks while the Er1Ag–0 glass demonstrates the characteristic absorption bands of Er^{3+} ions. The comparison of absorption spectrum of Er1Ag–0 glass specimen with that of Er0Ag–0 glass clearly unveils the existence of Er^{3+} ions in Er1Ag–0 glass. Furthermore, from Fig. 3, it is evident that the characteristic absorption peaks of Er^{3+} ions are also present in Ag NPs embedded glass specimens, which illustrates the presence of Er^{3+} ions in the Ag NPs embedded glass specimens too. Figure 3 displays that the spectra of $AgNO_3$-containing glasses exhibited a broad and robust peak at ~ 430 nm, which corresponds to the SPR of silver nanoparticles. It can also be identified that the SPR amplitude increases with the rise of $AgNO_3$ content due to the rise in the concentration of Ag NPs formed upon loading the more and more concentration of $AgNO_3$ in the composition [32]. Furthermore, from Fig. 3, it can be identified that the center of SPR peak has been slightly shifted towards longer wavelength with increase of Ag NPs concentration, which is manifested to growth of silver NPs routed in the glass hosts [22]. In addition, it is also manifested to increase of concentration of formation of Ag NPs occurred due to loading of more and more $AgNO_3$ in the glass composition [25, 33].

Usually, the amplitude of Er^{3+} absorption characteristic peaks is corroborated to asymmetry and covalency around the Er^{3+} ions and the rigidity of the glass is based on the hypothesis provided by Judd and Ofelt, famously referred to as Judd-Ofelt (JO) hypothesis [34, 35]. The JO parameters $\Omega_{t\ (t\ =\ 2,\ 4,\ 6)}$ computed from UV-Vis linear absorption results [25, 36] and quality factor (χ)

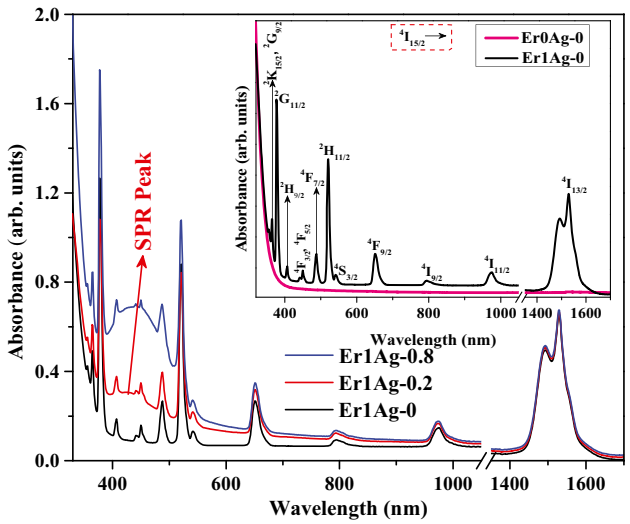

Fig. 3 Linear UV-Vis absorption spectral outcomes of Er1Ag–0, Er1Ag–0.2, and Er1Ag–0.8 glass samples, inset: absorption spectra of Er0Ag–0 and Er1Ag–0 glasses with assignment of Er^{3+} absorption peaks observed in Er1Ag–0 glass

are furnished in Table 1 for Er1Ag–0, Er1Ag0.2, and Er1Ag–0.8 glasses. From Table 1, it can be observed that the Ω_2 enhances with the increase of $AgNO_3$ content. This enhance effect in Ω_2 with the inclusion of more and more Ag NPs in the composition suggests that the trivalent erbium cations are occupied in strongly non-symmetric sites in the high amount of Ag NPs bearing glasses, which also instantiate that ligand field in erbium ions sorrounding is highly covalent in Ag NPs routed glasses [25]. Table 1 also shows the Ω_4 and Ω_6 increase with the rise of $AgNO_3$ quantity, which divulges that long-range structure related parameters (density and rigidity) of the glasses increases with the formation of Ag NPs in the glass system. This enhance behaviour of Ω_4 and Ω_6 also divulge that large Er^{3+} cations are dissolved in the glass matrix (solubility of Er^{3+} increases); thereby, the interionic separation with erbium ions decreases. This ultimately enhances the force of repulsion between surrounding similar Er^{3+} cations, thereby enhances the Ω_6 [25]. Furthermore, the χ of the studied glass specimens enhanced with the increase of $AgNO_3$ content, which indicates that a high concentration of Ag NPs routed glass matrix is beneficial for having high stimulated emission cross-section [18, 25, 27, 37, 38].

The PL emission spectral outcomes of Er1Ag–x glass samples are exhibited in Fig. 4 recorded for irradiation of 376 nm. The three PL emission lines evidenced at 538, 552, and 626 nm are related to $^2H_{11/2} \rightarrow {}^4I_{15/2}$, $^4S_{3/2} \rightarrow {}^4I_{15/2}$, and $^4F_{9/2} \rightarrow {}^4I_{15/2}$ transitions occurring within trivalent erbium ions, respectively. In Fig. 4, a weak PL signal has appeared at around 505 nm in addition to the PL emission peaks related to Er^{3+} ions. This weak PL signal and its intensity variation are not related to Er^{3+} ions, which might be related to the glass host or Ag NPs. In-depth structural and spectroscopic investigations are essential to address this, which will be a part of a future study. The $^4S_{3/2} \rightarrow {}^4I_{15/2}$ transition of Er^{3+} occurred at 552 nm is highly intense compared to other three PL emission lines. From Fig. 4 it can be noticed that emission intensity enhances with escalation of $AgNO_3$ content in the glass composition. In similar lines, the PL emission spectra in infrared region for all the glass specimens collected under the excitation of 980 nm are depicted in Fig. 5. All the glass specimens display a strong PL emission peak poisoned at 1535 nm owing to $^4I_{13/2} \rightarrow {}^4I_{15/2}$ inherent transition of Er^{3+}. The spectral results displayed in Fig. 5 divulge that intensity of PL emission lines improves with $AgNO_3$ content in the glass matrix. The luminescence improvement factor (LIF), defined as the ratio of PL emission intensity magnitude of Er^{3+} ions in NPs bearing glass to the NPs free glass. The LIF factors for green light transition are 1.15, 1.96, 2.57, and 2.79 for Er1Ag–0.2, Er1Ag–0.4, Er1Ag–0.6, and Er1Ag–0.8 glass samples, respectively. Similarly, for 1535 nm transition the magnitudes were found to be 1.54, 1.93, 2.42, and

Table 1 Judd–Ofelt intensity parameters and some spectroscopic magnitudes of examined glass specimens

Glass	$\Omega_{(t=2,4,6)}$ ($\times 10^{-20}$ cm^2)				$X = (\Omega_4/\Omega_6)$	σ_{emi} ($\times 10^{-21}$ cm^2)	FWHM (nm)	FWHM $\times$ σ_{emi} ($\times 10^{-26}$ cm^3)
	Ω_2	Ω_4	Ω_6	$\Sigma\Omega_t$				
Er1Ag–0	6.26	2.87	2.84	11.97	1.011	4.79	82.31	3.94
Er1Ag–0.2	7.96	3.05	3.01	14.02	1.013	5.92	95.62	5.66
Er1Ag–0.8	9.15	3.10	3.22	15.47	0.963	9.26	121.27	11.23

2.83 for Er1Ag–0.2, Er1Ag–0.4, Er1Ag–0.6, and Er1Ag–0.8 glass specimens, respectively. The increment of PL emission of erbum ions occurred in metallic Ag NPs routed glasses is because of the transfer of energy from metallic silver NPs to the corresponding energy levels of trivalent erbium ions and / or evinced local electric field produced by localized surface plasmons of Ag NPs [25].

The attenuations, such as an increase in the broadness and shift (towards red region) of maxima of the SPR band as seen in UV-Vis absorption results, expose the reduction in inter-particle distances (d_{Ag-Ag}) of silver NP and their subsequent growth with the increase of silver NPs quantity in the glass matrices. It has been documented that the diameter of the NPs and the separation between them are oppositely corroborated in the local field boost formula [22]. These variations clearly unveil the boosting of local electric field with increase of metallic silver NPs content in the glass host. Therefore, the improved attenuation noticed in PL properties with Ag^0 NPs is due to the boosted local field provoked metallic Ag NPs around the trivalent erbium ions [31]. Since, the boosted local field effectively enhances the rate of pumping of trivalent erbium ions to higher energy levels, which results in the high PL emission in different spectral regions depending the energy difference between the ground state and excited energy states of trivalent erbium ions [31].

In addition, when the metallic silver NPs routed glass host irradiated with electromagnetic radiation, the NPs routed in the glass host causes a weak emission which enhances the pumping rates of tripositive erbium ions to their excited energy levels. This boosted the photons content in upper energy levels of erbium ions [39]. Therefore, the energy transfer from metallic silver NPs to higher energy levels of erbium cations is contributory factor for the strong PL emission noticed for erbium ions PL peaks in Ag NPs routed glasses. Since the position of SPR peak of metallic silver lies very close to that of irradiated light utilized for recording

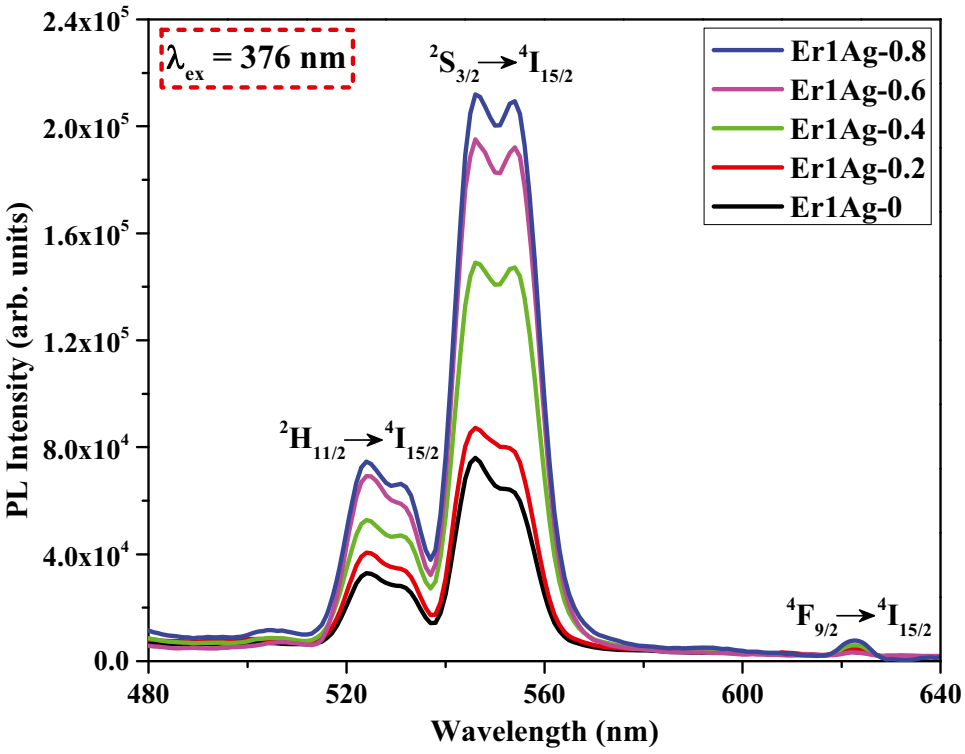

Fig. 4 The PL emission results of Er1Ag–*x* (where, *x* = 0, 0.2, 0.4, 0.6, and 0.8 mol % of $AgNO_3$) glasses in the visible region recorded with irradiation of 376 nm

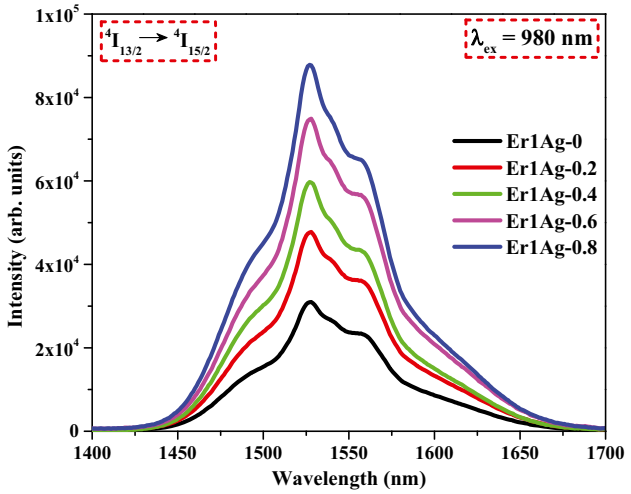

Fig. 5 The PL emission outcomes of Er1Ag–x (where, x = 0, 0.2, 0.4, 0.6, and 0.8 mol % of $AgNO_3$) glasses recorded in the infrared region with the irradiation of 980 nm

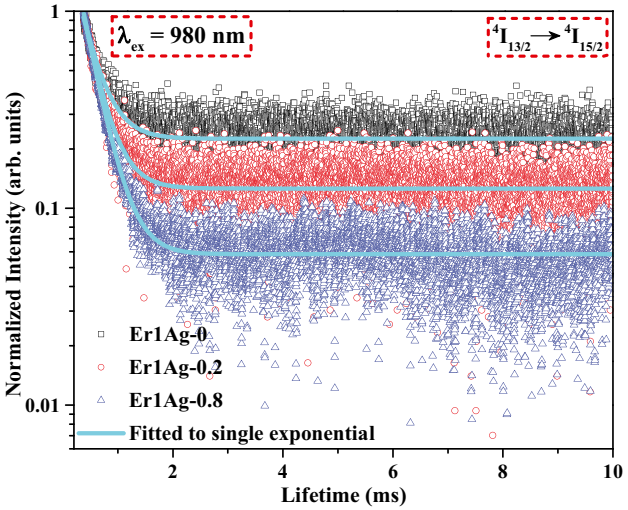

Fig. 6 Lifetime decay results of Er1Ag–x (x = 0, 0.2, and 0.8 mol % of $AgNO_3$) glasses collected with exposing the glasses for 980 nm wavelength light

the PL emission profiles in the visible region. Hence, it is believed that the transfer energy from metallic silver NPs to excited erbium ions energy levels is a highly acceptable origin contrast to the local field evinced origin for improved emission observed for visible spectra range.

The stimulated emission cross-section (σ_{emi}) [40] magnitudes were estimated for Er1Ag–0, Er1Ag–0.2, and Er1Ag–0.8 glass samples using corresoponding radiative properties and PL emission outcomes, and which are 4.79×10^{-21}, 5.92×10^{-21}, and 9.26×10^{-21} cm^2, respectively. The full width at half maximum (FWHM) factors computed from the PL emission spectral results, the results are 82.31, 95.62, and 121.27 nm respectively for Er1Ag–0, Er1Ag–0.2, and Er1Ag0.8 glass samples. The attenuation in these results clearly divulge that the formation of metallic Ag NPs in erbium ions activated glass hosts greatly boosts the emission cross-sections and bandwidths of PL emission lines of erbium ions in infrared spectral range. Furthermore, the gain bandwidth (FWHM$\times\sigma_{emi}$) factors are found to be 3.94, 5.66, and 11.23×10^{-26} cm^3 respectively for Er1Ag–0, Er1Ag–0.2, and Er1Ag–0.8 glass specimens. The greatness of gain bandwidth and related results noticed in the present study contrast to those achieved in other works [25, 27, 41] illustrate that the Er1Ag–0.8 glass host is largely suitable for fiber optic, photonic amplifier, and infrared laser functionalities.

The PL lifetime results for Er1Ag–0, Er1Ag–0.2, and Er1Ag–0.8 glass hosts recorded by monitoring $^4I_{13/2} \rightarrow {}^4I_{15/2}$ infrared emission transition with pumping of 980 nm are provided in Fig. 6 and all the outcomes were matched well with single exponential decay mechanism [27]. The decay lifetime (τ_{exp}) magnitudes were computed to be 2.54, 2.83, and 3.61 ms, respectively for Er1Ag–0, Er1Ag–0.2, and Er1Ag–0.0.8 glass samples. The τ_{exp} magnitudes boosted with silver NPs content in accordance with the PL emission intensity trend that noticed in infrared spectra region. This is corresponds to evinced local field stimulated by localized surface plasmons of metallic Ag NPs and energy transfer from Ag^0 NPs to the upper energy levels of tripositive erbium ions [25]. The quantum efficiency (η) factors were computed by following the procedure elaborated in the reference [25]. Table 2 furnishes the τ_{exp}, $\tau_{rad,}$ and η magnitudes for Er1Ag–0, Er1Ag–0.2, and Er1Ag–0.8 glass hosts and it unveil the increase behaviour with respect to Ag^0 NPs content in the host. The high quantum efficiency result achieved for Er1Ag–0.8 glass system divulge that this glass hosts is benefical for photonic and optoelectronic functionalities to execute their function in infrared spectral range [42, 43].

Summary

The Er^{3+} activated in borate glass specimens embedded with various concentrations of Ag NPs was synthesized by the standard melt–quench process. The XRD outcomes affirm the glassy nature of the glass samples examined in

Table 2 Lifetime and quantum efficiency magnitudes of examined glass specimens

Glass	τ_{exp} (ms)	τ_{rad} (ms)	η (%)
Er1Ag–0	2.54	2.91	87
Er1Ag–0.2	2.83	3.04	93
Er1Ag–0.8	3.55	3.58	99

the current investigation. The TEM micrograph divulged the presence of spherical-shaped Ag NPs with uniform distribution in the tested glass with a median size of 7.78 nm. The absorption outcomes further confirmed the existence of silver NPs by exhibiting the SPR peak in the spectra of the tested Ag NPs embedded glasses. The absorption results also unveiled the growth of silver NPs with an elevation of $AgNO_3$ content in the system. The PL emission intensity of both visible and infrared transitions is increased as the function of Ag NPs due to evinced local field provoked by localized surface plasmons of metallic Ag NPs and transfer of energy from metallic Ag NPs to corresponding energy levels of trivalent erbium ions. The maximum values of phenomenal parameters in the device fabrication mentioned in the Table 1 and η achieved for Er1Ag–0.8 glass divulge that a high concentration of silver NPs embedded glass specimens are beneficial for optical and optoelectronic functionalities.

Acknowledgements The authors express their gratitude to Princess Nourah bint Abdulrahman University Researchers Supporting Project number (PNURSP2022R57), Princess Nourah bint Abdulrahman University, Riyadh, Saudi Arabia.

Authors Contribution **Kempaiah Keshavamurthy**: conceptualization, data curation, writing—original draft and editing, **Gangareddy Jagannath**: methodology, conceptualization, formal analysis, writing—review and editing, **Dalal Abdullah Aloraini**: data curation, writing—review and editing, **Aljawhara H Almuqrin**: data curation, **M.I. Sayyed**: writing—review and editing, **K. N. Sathish**: writing—review and editing, and **P. Ramesh**: conceptualization, formal analysis, writing—review and editing.

Funding This research was funded by the Princess Nourah bint Abdulrahman University Researchers Supporting Project number (PNURSP2022R57), Princess Nourah bint Abdulrahman University, Riyadh, Saudi Arabia.

Research Data Policy and Data Availability The authors declare that the data supporting the findings of this study are available within the article. The raw data that support the findings are available on request from the corresponding author.

Declarations

Conflict of Interest The authors declare no competing interests.

References

1. Gushiken NK, Paganoto GT, Temperini MLA, Teixeira FS, Salvadori MC (2020) ACS Omega 5:10366–10373
2. Sendova M, Jiménez JA (2012) J Phys Chem C 116:17764–17772
3. Richter K, Campbell PS, Baecker T, Schimitzek A, Yaprak D, Mudring AV (2013) Phys Status Solidi 250:1152–1164
4. Malekzad H, Sahandi Zangabad P, Mirshekari H, Karimi M, Hamblin MR (2017) Nanotechnol Rev 6:301–329
5. Han X, Xu K, Taratula O, Farsad K (2019) Nanoscale 11:799–819
6. Camelio S, Babonneau D, Vandenhecke E, Louarn G, Humbert B (2021) Nanoscale Adv 3:6719–6727
7. Kumar P, Mathpal MC, Prakash J, Jagannath G, Roos WD, Swart HC (2020) Mater Res Bull 125:110799
8. Da Silva DS, De Assumpção TAA, Kassab LRP, De Araújo CB (2014) J Alloys Compd 586:S516–S519
9. Jagannath G, Eraiah B, Jayanthi K, Keshri SR, Som S, Vinitha G, Pramod AG, Krishnakanth KN, Devarajulu G, Balaji S, Rao SV, Annapurna K, Das S, Allu AR (2020) Phys Chem Chem Phys 22:2019–2032
10. Som T, Karmakar B (2010) Plasmonics 5:149–159
11. De Araújo CB, Kassab LRP (2016) in: Glas. Nanocomposites Synth Prop Appl pp 131–144
12. Wu Y, Shen X, Dai S, Xu Y, Chen F, Lin C, Xu T (2011) J Phys Chem C 115:25040–25045
13. Liu J, Wang Q, Sang X, Hu H, Li S, Zhang D, Liu C, Wang Q, Zhang B, Wang W, Song F (2021) Nanomaterials 11:1037
14. Li J, Wei R, Liu X, Guo H (2012) Opt Express 20:10122–10127
15. Malta OL, Santa-Cruz PA, Desa GF, Auzel F (1985) J Lumin 33:261–272
16. Mariano D, Reyes L, Kassab P, Lüthi SR, De Araújo CB, Anderson SL, José M, Bell V (2007) Appl Phys Lett 90:081913
17. Dousti MR, Sahar MR, Ghoshal SK, Amjad RJ, Arifin R (2013) J Mol Struct 1033:79–83
18. Qi J, Xu T, Wu Y, Shen X, Dai S, Xu Y (2013) Opt Mater 35:2502–2506
19. Soltani I, Hraiech S, Horchani-Naifer K, Massera J, Petit L, Férid M (2016) J Non Cryst Solids 438:67–73
20. Rajaramakrishna R, Ruangtaweep Y, Sangwaranatee N, Kaewkhao J (2019) J Non Cryst Solids 521:119522
21. Gao G, Wei J, Shen Y, Peng M, Wondraczek L (2014) J Mater Chem C 2:8678–8682
22. Fatima N, Pramod AG, Jagannath G, Rajaramakrishna R, Keshavamurthy K, Ramesh P, Sathish KN, Alhuthali AMS, Sayyed MI, Hegde V, Rao SV, Nadaf YF (2021) Ceram Int 47:16801–16808
23. Ramesh P, Gangareddy J, Sathish KN, Pramod AG, Hegde V, Pasha UM, Khan S, Annapurna K, Sayyed MI, Alhuthali AMS, Agarkov DA, Kokila MK (2021) Opt Mater 114:110933
24. Sasai J, Hirao K (2001) J Appl Phys 89:4548
25. Fares H, Elhouichet H, Gelloz B, Férid M (2014) J Appl Phys 116:123504
26. Gelija D, Kadathala L, Borelli DPR (2018) Opt Mater 78:172–180
27. Swetha BN, Devarajulu G, Keshavamurthy K, Jagannath G, Deepa HR (2021) J Alloys Compd 856:158212
28. Manzani D, Marega E, Nunes LAO, Osorio SPA, Rivera VAG, Ledemi Y, Messaddeq Y (2010) Opt Express 18:25321–25328
29. Rivera VAG, Ledemi Y, Osorio SPA, Manzani D, Ferri FA, Ribeiro SJL, Nunes LAO, Marega E (2013) J Non Cryst Solids 378:126–134
30. Qi Y, Zhou Y, Wu L, Yang F, Peng S, Zheng S, Yin D (2014) J Lumin 153:401–407
31. Som T, Karmakar B (2009) J Appl Phys 105(1–8):013102
32. Gangareddy J, Bheemaiah E, Gandhiraj V, James JT, Jose JK, Katturi Naga K, Soma VR (2018) Appl Phys B Lasers Opt 124
33. Jagannath G, Eraiah B, NagaKrishnakanth K, Rao SV (2018) J Non Cryst Solids 482:160–169
34. Judd BR (1962) Phys Rev 127:750–761
35. Ofelt GS (1962) J Chem Phys 37:511–520
36. Serqueira EO, De Morais RF, Dantas NO (2013) J Alloys Compd 560:200–207
37. Yang J, Dai S, Zhou Y, Wen L, Hu L, Jiang Z (2002) J Appl Phys 93:977
38. Jlassi I, Elhouichet H, Ferid M, Barthou C (2010) J Lumin 130:2394–2401

39. Mechergui I, Fares H, Mohamed SA, Nalin M, Elhouichet H (2017) J Lumin 190:518–524
40. OSA Tech. Dig. (Optica Publ. Group, 1990) (1990)
41. Fares H, Stambouli W, Elhouichet H, Gelloz B, Férid M (2016) RSC Adv 6:31136–31145
42. Caetano M, Silva ACA, Filho JCS, De Morais RF, Sales TO, Andrade AA, Dantas NO (2020) J Lumin 228:117599
43. Aouaini F, Maaoui A, Mohamed NBH, Alanazi MM, El Maati LA (2022) J Alloys Compd 894:162506